Non-linear Effects in Plasmas

May 9, 2016

Abstract

A particle-in-cell code is developed and used to test efficacy of magnetic confinement. The program allows visualisation of electromagnetic fields and their source terms. The particles' velocity distribution function is measured relative to a Maxwellian distribution. A solver is written using OpenFOAM for magnetohydrodynamic equations in the thermal limit. The theory behind non-linear theory set out by Tsytovich (1970) is expounded using the current density as an example. Finally the Landau treatment of non-linear effects is presented and applied to demonstrate damping of plasma waves.

Contents

1 Introduction

When analysing complex plasma phenomena it can be elucidating to simulate them numerically. In this project, two such simulators are produced, each with their own merits. A particle-in-cell code approaches the problem in an atomistic direction, while a magnetohydrodynamics solver employs continuum mechanics. These methods are both tested out on a range of scenarios. Finally non-linear kinetics are analysed in detailed theory, using approaches from Tsytovich and Landau.

1.1 Literature Review

A modern beginner text for plasma physics is Goldston and Rutherfords *Introduction to Plasma Physics*[4]. It covers a broad range and is a useful starting point for most topics. The original inspiration for this project comes from Tsytovich's *Nonlinear Effects in Plasma*[12] and the accompanying lectures[11]. Together these cover non-linear and induced processes including scattering, turbulence and damping. *The Particle Kinetics of Plasmas*[16] is a comprehensive study of kinetic theory, with an introduction to magnetohydrodynamics. Mitchner and Kruger's *Partially Ionised Gases*, also has thorough analysis of this area. The particle-in-cell model has had a resurgence at the turn of the millennium with the development of new charge conservation methods, in particular Esirkepov[19] and Umeda et al.[17]. These new works build on the established foundations developed amongst others by Boris[3] and Yee[18].

Part I
Computation

There are three commonly accepted mathematical descriptions of plasma. The particle model is the most accurate one can be without making quantum corrections, but it is useless at describing collective phenomena and better suited to analysing the microscopic phenomena such as collisions. The fluid model is simpler to implement, but is limited in its scope to Maxwellian distributions, and therefore is not suitable when collisions are infrequent. For these cases the kinetic theory, in which the key object is the six-dimensional distribution function $f(\mathbf{x}, \mathbf{v}, t)$ is required. Kinetic theory leads to some important theoretical results, but is rarely used in computational simulations.

2 Particle-In-Cell

The particle-in-cell model is an attempt to make the particle approach more tractable by discretising the domain and reducing the number of particles. A PIC code was built and tested against some known theoretical results.

2.1 Particles

It is not feasible to simulate using $\mathcal{O}(N_A)$ particles so in all particle-based computations they are grouped into finite sized superparticles. This approximation uses the assumption that particles initially close together in phase space will evolve in a similar way. At large distances the interaction between two superparticles is the same as for two equivalent point particles, however at short distances where the superparticles start to overlap the interaction is weaker because the region of overlap does not contribute. Having a weakened short range interaction is advantageous because it means the dynamics are smooth at even at low number density[8]. Attributed to each superparticle are shape functions $S_x(x - x_p(t))$ and $S_v(v - v_p(t))$. These are compact functions which describe the arrangement of particles' position and velocity within a superparticle. S_v is usually defined as the Dirac delta so all components of the superparticle have the same velocity. The first order spatial shape function at a lattice point is:

$$S_i(\xi) = \begin{cases} 1 - |\xi - i| & \text{if } |\xi - i| < 1 \\ 0 & \text{otherwise} \end{cases} \tag{2.1}$$

where i is the index of the lattice point.

2.1.1 Boris Algorithm

Once the fields are solved at the particles' positions, their motion can be integrated to find their next position. The standard PIC integrator is the Boris algorithm. While only a second order integrator, unlike higher order schemes such as RK4, the Boris scheme conserves phase space volume[13]. This means that it can be used for an arbitrary number of time steps without a drift in energy since the energy error is bounded for all time steps. Conversely RK4 will have poor long term fidelity because the energy errors add coherently at each

step, even though they are smaller. The Boris method is similar to the leapfrog method except it includes an intermediate rotation to account for the velocity dependence of the magnetic force. The steps in the algorithm are:

$$\mathbf{v}_- = \mathbf{v}_{i-1/2} + \frac{q\mathbf{E}}{m}\frac{\Delta t}{2} \tag{2.2}$$

$$\mathbf{v}' = \mathbf{v}_- + \mathbf{v}^- \times \mathbf{t} \tag{2.3}$$

$$\mathbf{v}_+ = \mathbf{v}_- + \mathbf{v}' \times \mathbf{s} \tag{2.4}$$

$$\mathbf{v}_{i+1/2} = \mathbf{v}_+ + \frac{q\mathbf{E}}{m}\frac{\Delta t}{2} \tag{2.5}$$

$$\mathbf{x}_{i+1} = \mathbf{x}_i + \Delta t \mathbf{v}_{i+1/2} \tag{2.6}$$

where

$$\mathbf{t} = \frac{q\mathbf{B}}{m}\frac{\Delta t}{2} \tag{2.7}$$

$$\mathbf{s} = \frac{2\mathbf{t}}{1+t^2} \tag{2.8}$$

2.1.2 Field Interpolation

The fields defined on the mesh sites must be interpolated to the particle positions. To conserve energy this must be done using the same weighting functions as the current deposition:

$$\mathbf{E}(\mathbf{x}) = \sum_i \mathbf{E}_i S_i(\mathbf{x}) \tag{2.9}$$

where the sum is over all lattice points (although in practice only ones adjacent to the particle will contribute).

2.2 Grid

While particle motion is allowed over a continuous domain, the electromagnetic fields and source terms are defined on a discrete grid to reduce the number of particle interaction terms from $\sim N^2_{particle}$ to $\sim \alpha N_{particle} + \beta N_{cell}$.

2.2.1 Yee Cells

Electric and magnetic fields are defined at offset points so that Maxwell's equations can be solved discretely. The convention used here is that elctric fields and current densities are defined along cell edges, magnetic fields are defined on cell faces and charge densities are defined on cell vertices. This arrangement comprises a Yee cell[18]

2.2.2 Deposition

A naive way to deposit currents onto the lattice points is simply to weight the charge fluxes from each particle by area i.e:

$$J^i = \frac{1}{\Delta V}\sum_{n=1}^{N_p} q_n v_n^i S\left(\frac{x_n}{\Delta x}\right) S\left(\frac{y_n}{\Delta y}\right) S\left(\frac{z_n}{\Delta z}\right) \tag{2.10}$$

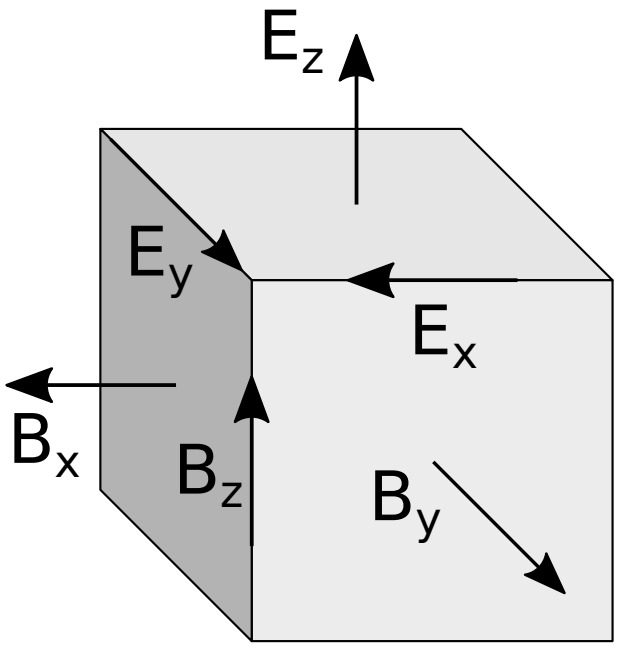

Figure 1: A single Yee cell. By offsetting the field components a discretised vector calculus can be performed.

where ΔV is the cell volume $\Delta x \Delta y \Delta z$ and each S is defined at the appropriate offset defined by the Yee cell. However, it can be shown that this does not perfectly conserve charge. There are several ways to correct this problem, of which the zig-zag scheme by Umeda et al.[17] is accurate and efficient. A particle's motion in each time step is decomposed into two segments with an intermediate relay point such that each segment is entirely contained within a cell. The charge flux from each segment is then weighted and deposited on the relevant lattice points. The efficiency of the algorithm comes from its method for calculating the coordinates of the relay point without *if* statements. In 3D the relay point's coordinates are:

$$x_r^i = min\left\{min\left(I_1^i \Delta x^i, I_2^i \Delta x^i\right), max\left[max\left(I_1^i \Delta x^i, I_2^i \Delta x^i\right), \frac{x_1^i + x_2^i}{2}\right]\right\} \tag{2.11}$$

The two flux densities are:

$$\mathbf{f}_1 = q\frac{\mathbf{x}_r - \mathbf{x}_1}{\Delta V \Delta t} \tag{2.12}$$

$$\mathbf{f}_2 = q\frac{\mathbf{x}_2 - \mathbf{x}_r}{\Delta V \Delta t} \tag{2.13}$$

Each flux density f_l for $l = 1, 2$ is then deposited on the relevant grid point:

$$J_x\left(i_l+\frac{1}{2},j_l,k_l\right)=f_{xl}\left(1-W_{yl}\right)\left(1-W_{zl}\right) \tag{2.14}$$

$$J_x\left(i_l+\frac{1}{2},j_l+1,k_l\right)=f_{xl}W_{yl}\left(1-W_{zl}\right) \tag{2.15}$$

$$J_x\left(i_l+\frac{1}{2},j_l,k_l+1\right)=f_{xl}\left(1-W_{yl}\right)W_{zl} \tag{2.16}$$

$$J_x\left(i_l+\frac{1}{2},j_l+1,k_l+1\right)=f_{xl}W_{yl}W_{zl} \tag{2.17}$$

and cyclic permutations. The weight functions are defined in terms of the shape function (2.1):

$$W_{al}=S_{i_{al}}\left(\frac{x_{al}+x_{ra}}{2\Delta x_a}\right) \tag{2.18}$$

2.2.3 FDTD method

A finite-difference time-domain (FDTD) method can be used on Maxwell's equations. Defining the operators:

$$\nabla^+ f_{i,j,k}=\left(\frac{f_{i+1,j,k}-f_{i,j,k}}{dx},\frac{f_{i,j+1,k}-f_{i,j,k}}{dy},\frac{f_{i,j,k+1}-f_{i,j,k}}{dz}\right) \tag{2.19}$$

$$\nabla^- f_{i,j,k}=\left(\frac{f_{i,j,k}-f_{i-1,j,k}}{dx},\frac{f_{i,j,k}-f_{i,j-1,k}}{dy},\frac{f_{i,j,k}-f_{i,j,k-1}}{dz}\right) \tag{2.20}$$

the fields for time step n are given by (2.21) and (2.22). This algorithm automatically preserves the continuity equation and the divergenceless of $\mathbf{B}$ if they are satisfied in the initial configuration.

$$\mathbf{B}^n=\mathbf{B}^{n-1/2}-\left(\nabla^-\times\mathbf{E}^n\right)dt \tag{2.21}$$

$$\mathbf{E}^{n+1}=\mathbf{E}^n\left(\nabla^+\times\mathbf{E}^n-\mathbf{J}^{n+1/2}\right)dt \tag{2.22}$$

2.2.4 Whole algorithm

The process undertaken in each time step of a PIC computation is therefore[14]:

1. Update $\mathbf{B}^{n-1/2}$ to $\mathbf{B}^n$ using (2.21)
2. Advance $\mathbf{v}^{n-1/2}$ to $\mathbf{v}^{n+1/2}$ and $\mathbf{x}^n$ to $\mathbf{x}^{n+1}$ using (2.2)
3. Compute $\mathbf{J}^{n+1/2}$ (2.11) - (2.1)
4. Update $\mathbf{B}^n$ to $\mathbf{B}^{n+1/2}$ using (2.21)
5. Update $\mathbf{E}^n$ to $\mathbf{E}^{n+1}$ using (2.22)

2.3 Environment

External objects can be added which act on the particles. Their action on the particles is calculated based on the position of the particle and added to the effect from the grid.

2.3.1 Coils

Circular coils produce a magnetic field; it is possible to arrange coils in a way such that a fraction of the plasma is contained by the field produced. The off-axis field in polar coordinates for a coil radius a centred on the origin pointing in the z direction is[9]:

$$B_z = B_0 \frac{1}{\pi\sqrt{Q}} \left[\frac{1-\alpha^2-\beta^2}{Q-4\alpha} E\left(\sqrt{\frac{4\alpha}{Q}}\right) + K\left(\sqrt{\frac{4\alpha}{Q}}\right) \right] \tag{2.23}$$

$$B_r = B_0 \frac{\gamma}{\pi\sqrt{Q}} \left[\frac{1+\alpha^2+\beta^2}{Q-4\alpha} E\left(\sqrt{\frac{4\alpha}{Q}}\right) - K\left(\sqrt{\frac{4\alpha}{Q}}\right) \right] \tag{2.24}$$

with:
$Q = (1+\alpha)^2 + \beta^2 \quad \alpha = \frac{r}{a} \quad \beta = \frac{x}{a} \quad \gamma = \frac{x}{r} \quad B_0 = \frac{\mu_0 N I}{2a}$
$K(k)$ and $E(k)$ are the complete elliptic integrals of the first and second kind:

$$K(k) = \int_0^{\frac{\pi}{2}} \frac{d\theta}{\sqrt{1-k^2\sin^2\theta}} \tag{2.25}$$

$$E(k) = \int_0^{\frac{\pi}{2}} \sqrt{1-k^2\sin^2\theta}\, d\theta \tag{2.26}$$

2.4 Implementation

The code was developed in modern *C++* in an object-oriented programming style. It was designed to be flexible and efficient.

2.5 Magnetic Bottle

A charged particle moving in a magnetic field will undergo helical motion around the magnetic field lines due to the Lorentz force $\mathbf{F} = q\mathbf{v} \times \mathbf{B}$. The velocity of a single particle can be decomposed into components perpendicular and parallel to the magnetic field. The magnetic moment is found to be constant[7]:

$$\frac{d\mu}{dt} = \frac{d}{dt}\left(\frac{mv_\perp^2}{2B}\right) = 0 \tag{2.27}$$

The force on a particle due to the magnetic field gradient can be shown to be $\mathbf{F}_\parallel = -\frac{mv_\perp^2}{2B}\nabla_\parallel B$, however we will use an energy argument.

2.5.1 Confinement Ratio

In terms of components parallel and perpendicular to the magnetic field, the kinetic energy is:

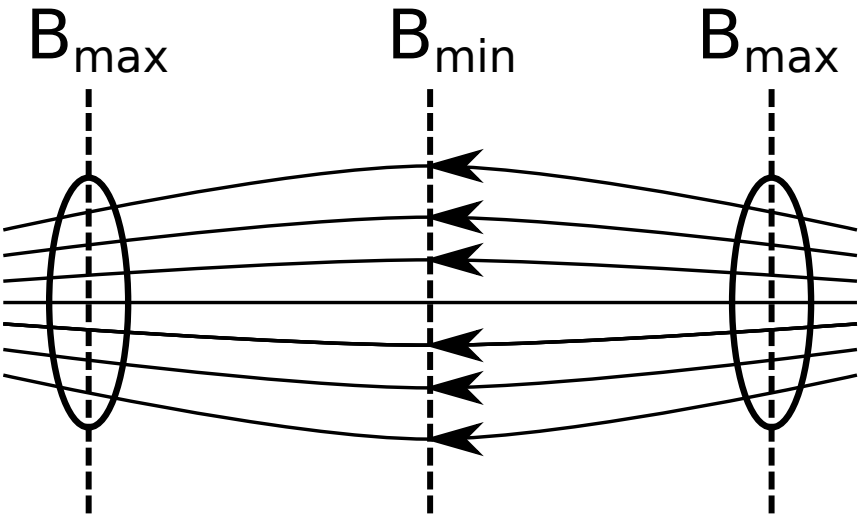

Figure 2: Two coils can create a magnetic field gradient, which can confine a fraction of particles to the space between the coils.

$$E = \frac{1}{2}mv_{\parallel}^2 + \frac{1}{2}mv_{\perp}^2 = \frac{1}{2}mv_{\parallel}^2 + \mu B \tag{2.28}$$

E and μ are constant, so the velocity at the points labelled B_{min} and B_{max} are:

$$\left(v_{\parallel}^2\right)_{max} = \frac{2}{m}\left(E - \mu B_{min}\right) \quad (2.29) \qquad \left(v_{\parallel}^2\right)_{min} = \frac{2}{m}\left(E - \mu B_{max}\right) \quad (2.30)$$

For a particle to be trapped $E \leq \mu B_{max}$. Using (2.27) the ratio between the speed components at the midpoint is[7]:

$$\left(\frac{v_{\parallel}^2}{v_{\perp}^2}\right)_{mid\text{-}plane} \leq \frac{B_{max}}{B_{min}} - 1 \tag{2.31}$$

Particles which are trapped have velocities lying outside the two 'loss cones' formed by the polar angles θ_0 and $\pi - \theta_0$

$$\theta_0 = \arcsin\sqrt{\frac{B_{min}}{B_{max}}} \tag{2.32}$$

Calculating the fraction of an initially isotropic distribution of particles at the mid-plane which are trapped by the bottle gives:

$$f_{trap} = \cos\theta_0 = \sqrt{1 - \frac{B_{min}}{B_{max}}} \tag{2.33}$$

We used the PIC code developed to explore a range of f_{trap} and see how well (2.33) holds by counting the number of particles for which (2.5.1) holds. The environment used is as follows:

- Five parallel solenoidal coils with equal radius and spacing

- Two end cap coils with variable radius
- An initial distribution of Maxwellian charged particles, uniformly distributed over the disc at the mid-plane inside the middle coil

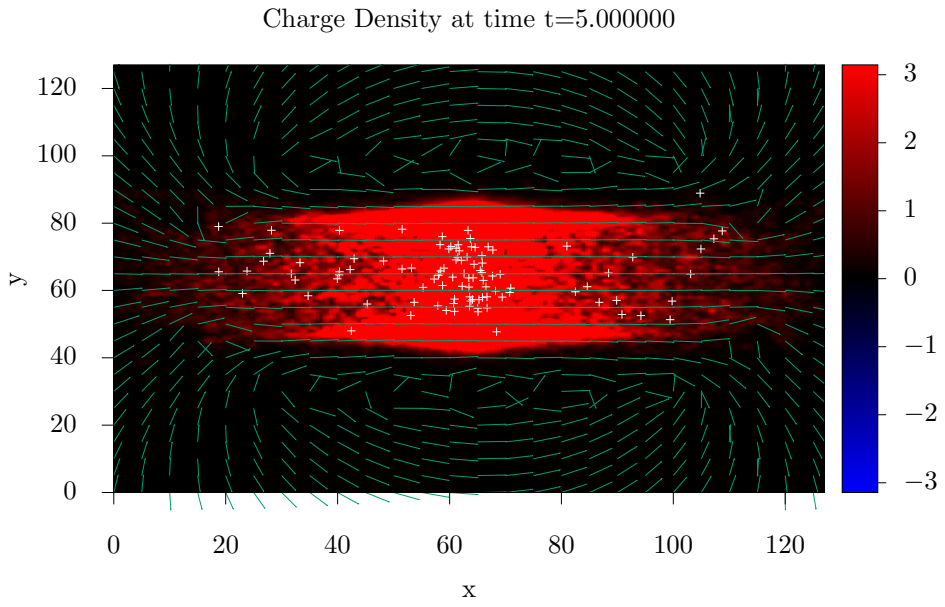

Figure 3: Demonstration of the PIC code for the environnment described above. The green arrows show the magnetic field generated by the coils. The confinement is greatest in the centre of the solenoid

2.6 Velocity Distribution

It has been shown[20] that a distribution is normal if the statistic:

$$v_n(1) = \log\left(\left|\hat{\phi}_S(1)\exp(1/2)\right|\right) = 0 \tag{2.34}$$

where $\hat{\phi}_S(t)$ is the ecf. We test this relation for a plasma initially at rest

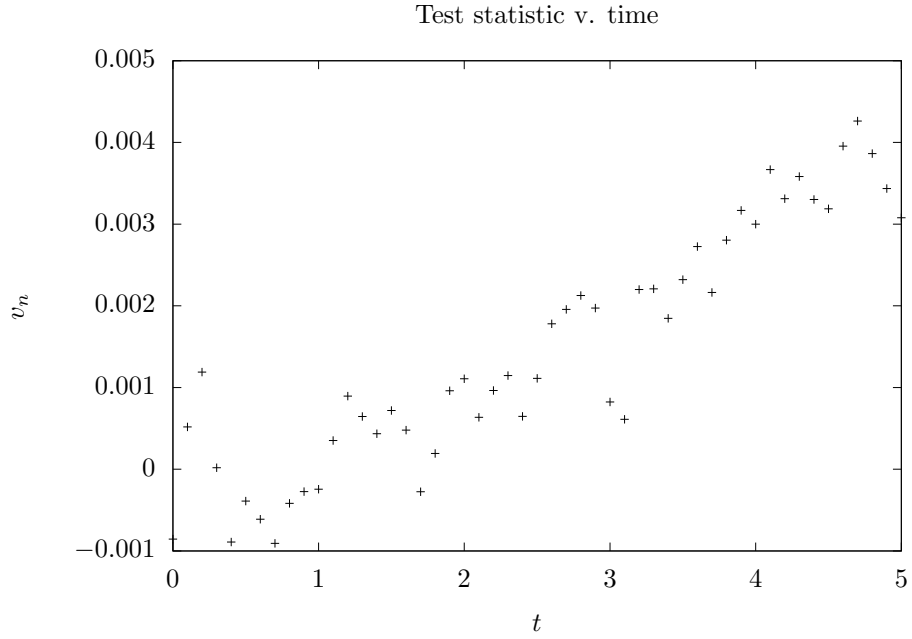

Figure 4: The test statistic fluctuates around zero although there is a slight upward trend as the particle distribution function drifts away from Maxwellian. $100,000$ particles were used

3 Magnetohydrodynamics

The fluid model of plasma is also called magnetohydrodynamics (MHD) because it is based around adapting the Eulerian fluid equations to include electromagnetism.

3.1 MHD equations

For simplicity the following treatment considers a plasma consisting of equal numbers of electrons and a single species of singly charged ion. The single-fluid magnetohydrodynamic model is obtained by combining the constituent species' number densities (which are assumed to be approximately identical) into mass and charge densities[4]:

$$\rho = n_i M + n_e m \approx nM \tag{3.1}$$

$$\sigma = e\left(n_i - n_e\right) \tag{3.2}$$

A velocity field and current density can also be defined:

$$\mathbf{u} = \frac{n_i M \mathbf{u}_i + n_e m \mathbf{u}_e}{\rho} \approx \mathbf{u}_i + \frac{m}{M}\mathbf{u}_e \tag{3.3}$$

$$\mathbf{j} = e\left(n_i \mathbf{u}_i - n_e \mathbf{u}_e\right) \approx ne\left(\mathbf{u}_i - \mathbf{u}_e\right) \tag{3.4}$$

The continuity of mass equation for the mass density is:

$$\frac{d\rho}{dt} = \frac{\partial \rho}{\partial t} + \nabla \cdot (\rho \mathbf{u}) = 0 \tag{3.5}$$

Charge conservation must also be obeyed:

$$\frac{d\sigma}{dt} = \frac{\partial \sigma}{\partial t} + \nabla \cdot \mathbf{j} = 0 \tag{3.6}$$

Momentum conservation for a compressible fluid is given by[15]

$$\frac{\partial}{\partial t}(\rho \mathbf{u}) + \nabla \cdot (\rho \mathbf{u} \otimes \mathbf{u}) - \nabla \cdot \left[\mu \left(\nabla \mathbf{u} + (\nabla \mathbf{u})^T \right) - \frac{2}{3} \mu (\nabla \cdot \mathbf{u}) \mathbb{1} \right] = -\nabla p + \sigma \mathbf{E} + \mathbf{j} \times \mathbf{B} \tag{3.7}$$

Energy conservation for a fluid in an electromagnetic field is given by:

$$\frac{d\rho e}{dt} + \frac{d}{dt}\left(\frac{\rho |\mathbf{u}|^2}{2} \right) + \frac{dU}{dt} - \nabla \cdot \left(\frac{k}{C_v} \right) \nabla e = p \nabla \cdot \mathbf{u} \tag{3.8}$$

with $e = C_v T$ and Fourier's Law $\mathbf{q} = -k \nabla T$ giving the heat flow. U is the electromagnetic energy:

$$U = \frac{\epsilon_0 |\mathbf{E}|^2}{2} + \frac{|\mathbf{B}|^2}{2\mu_0} \tag{3.9}$$

The current in a plasma is given by a quasi-Ohmic law[15][4]:

$$\mathbf{j} = \sigma_m \left(\underbrace{\mathbf{E}}_{\text{Electric current}} + \underbrace{\mathbf{u} \times \mathbf{B}}_{\text{Induction current}} - \underbrace{\frac{\mathbf{j} \times \mathbf{B} - \nabla p}{ne}}_{\text{Hall current}} \right) \tag{3.10}$$

It will be shown that the Hall current can be neglected when the quasi-neutrality approximation holds.
These equations together with Maxwell's equations[1]form single-fluid magneto-hydrodynamics, but are incomplete. For completion, an equation of state is required.

3.1.1 Quasi-Neutrality Approximation

It is assumed that a plasma is globally neutral, and therefore that the charge density at any given point is in some way small. In (3.7), comparing the $\sigma \mathbf{E}$ term with the inertial term $\rho \mathbf{u} \cdot \nabla \mathbf{u}$ with (3.14) gives[4]:

$$\frac{\sigma \mathbf{E}}{\rho \mathbf{u} \cdot \nabla \mathbf{u}} \sim \frac{\epsilon_0 E^2 / L}{\rho u^2} \sim \frac{\epsilon_0 B^2}{\rho} \tag{3.15}$$

[1]for reference

$$\nabla \times \mathbf{B} = \mu_0 \mathbf{j} + \frac{1}{c^2} \frac{\partial \mathbf{E}}{\partial t} \tag{3.11}$$

$$\nabla \times \mathbf{E} = -\frac{\partial \mathbf{B}}{\partial t} \tag{3.12}$$

$$\nabla \cdot \mathbf{B} = 0 \tag{3.13}$$

$$\nabla \cdot \mathbf{E} = \frac{\sigma}{\epsilon_0} \tag{3.14}$$

It has been assumed that $u \sim E/B$. The dimensionless quantity $\frac{\epsilon_0 B^2}{\rho}$ is small ($\sim 10^{-2} - 10^{-3}$) in all plasmas that will be considered. Therefore the electric field term in the momentum balance equation can be ignored:

$$\frac{\partial}{\partial t}(\rho \mathbf{u}) + \nabla \cdot (\rho \mathbf{u} \otimes \mathbf{u}) - \nabla \cdot \left[\mu \left(\nabla \mathbf{u} + (\nabla \mathbf{u})^T \right) - \frac{2}{3} \mu (\nabla \cdot \mathbf{u}) \mathbb{1} \right] = -\nabla p + \mathbf{j} \times \mathbf{B} \tag{3.16}$$

A similar treatment allows the omission of $\frac{\partial \sigma}{\partial t}$ in (3.6) and the displacement current in (3.11):

$$\nabla \cdot \mathbf{j} = 0 \tag{3.17}$$

$$\nabla \times \mathbf{B} = \mu_0 \mathbf{j} \tag{3.18}$$

3.1.2 Larmor Radius

A comparison of the Hall and inductance currents in (3.10) gives[4]:

$$\frac{\mathbf{j} \times \mathbf{B} - \nabla p}{ne\mathbf{u} \times \mathbf{B}} \sim \frac{T}{euBL} \sim \frac{Mv_{t,i}^2}{euBL} \sim \frac{Mv_{t,i}}{eBL} \sim \frac{v_{t,i}}{\omega_{ci} L} \sim \frac{r_{Li}}{L} \tag{3.19}$$

where the first step assumes the $\rho \mathbf{u} \cdot \nabla \mathbf{u}$, $\mathbf{j} \times \mathbf{B}$ and ∇p terms are of the same order i.e. inertial, pressure-driven and electromagnetic forces are all equally important. The remaining steps assume the ideal gas law $p \sim nT$ and the assumption that the velocity is approximately the thermal velocity $u \sim v_{t,i} \sim (T/M)^{1/2}$. It is therefore justified to omit the Hall current in (3.10) when the length scale is small compared to the length scale of the plasma[2]:

$$\mathbf{j} = \sigma_m (E + \mathbf{u} \times \mathbf{B}) \tag{3.20}$$

3.2 Transport

The solver requires thermodynamic and transport properties of the system. Many of these can be calculated by considering the collision rates of the species in the plasma.

3.2.1 Electrical Conductivity

In equilibrium, the quasi-Ohm's Law (3.20) can be reduced simply to $\mathbf{j} = \sigma_m \mathbf{E}$. Consider the equation of motion for the electrons:

$$mn_e \frac{d\mathbf{u}_e}{dt} = -n_e \mathbf{E} + \mathbf{R}_{ei} \tag{3.21}$$

The last term is the momentum transferred to the electrons by ions $\mathbf{R}_{ei} = -mn_e \langle \nu_{ei} \rangle (\mathbf{u}_e - \mathbf{u}_i) = \frac{m}{e} \langle \nu_{ei} \rangle \mathbf{j}$ where $\langle \nu_{ei} \rangle$ is the electron-ion collision frequency averaged over the velocity distribution. In equilibrium by comparing Ohm's Law with (3.21), the conductivity is found to be[4] [10]:

[2]The characteristic length scale of the plasma is the vaguely defined distance over which the pressure changes. One quantity which $\sim L$ is the wavelength of Langmuir waves.

$$\sigma_m = \frac{n_e e^2}{m \langle \nu_{ei} \rangle} \tag{3.22}$$

The electron-ion cross-section for Coulomb collisions is:

$$\sigma_{ei} = \frac{Z^2 e^4 \ln \Lambda}{4\pi \epsilon_0^2 m^2 u^4} \tag{3.23}$$

The factor of $\ln \Lambda$ is a renormalisation to cut-off the otherwise divergent integral over impact parameters by introducing a maximum impact parameter b_max with $\Lambda = b_{max}/b_0$. b_0 is defined here as the distance at which an electron's kinetic energy is twice its potential energy[3]. Coulomb interacton is shielded above the Debye length $\lambda_D = \left(\epsilon_0 T_e / n_e e^2\right)^{1/2}$, so this can be taken as b_{max}. Therefore $\Lambda \sim n\lambda_D^3$ is by definition large. Typically $\ln \Lambda$ is about 20. From the definition of cross-section $\nu_{ei} = n_i \sigma_{ei} \langle u_{rel} \rangle$, the collisional frequency is:

$$\nu_{ei}(u) = \frac{Z^2 e^4 n_i \ln \Lambda \langle u \rangle}{4\pi \epsilon_0^2 m^2 u^3} \tag{3.24}$$

Considering collisions with a drifting Maxwellian distribution, the total collision rate over the whole distribution is:

$$\langle \nu_{ei} \rangle = \frac{4}{3\sqrt{\pi}} \nu_{ei} \left(\sqrt{\frac{3k_B T}{m}} \right) = \frac{2^{1/2} n_i Z^2 e^4 \ln \Lambda}{12\pi^{3/2} \epsilon_0^2 m^{1/2} T_e^{3/2}} \tag{3.25}$$

The conductivity can now be written:

$$\sigma_m = \frac{12\pi^{3/2} \epsilon_0^2 m^{1/2} T_e^{3/2}}{2^{1/2} Z e^2 \ln \Lambda} \tag{3.26}$$

3.2.2 Dynamic Viscosity

By considering mass continuity and the definition of shear stress as a rate of momentum flux[4]it can be shown that the dynamic viscosity can be written as[1]:

$$\mu = \frac{1}{3} \rho \lambda \langle u \rangle = \frac{M \langle u \rangle \langle u_{rel} \rangle}{3 \langle \nu_{ii} \rangle} = \frac{\sqrt{2} M \langle u \rangle^2}{3 \langle \nu_{ii} \rangle} \tag{3.27}$$

where λ is the mean free path and a Maxwellian distribution has been assumed. The ion-ion collision rate can be obtained the same way as (3.25), except there is a factor of $\sqrt{2}$ different to account for the reduced mass of the ion-ion system:

$$\langle \nu_i \rangle = \frac{n_i Z^4 e^4 \ln \Lambda}{12\pi^{3/2} \epsilon_0^2 M^{1/2} T_i^{3/2}} \tag{3.28}$$

[3] $b_0 = \frac{Ze^2}{4\pi\epsilon_0 m u^2}$

[4] For a Newtonian fluid, dynamic viscosity is the ratio of shear stress to a velocity gradient: $\tau = \mu \frac{du_x}{dy}$

3.3 Implementation

To make the custom solver, a prebuilt solver *buoyantpimpleFoam* was adapted. *buoyantpimpleFoam* already solves (3.5), (3.7) and (3.8) without their respective electromagnetic terms. It is therefore simple to add these terms to the relevant parts of the solver, as well as (3.12), (3.13), (3.14), (3.18) and (3.20) for a full description. These equations can be represented in a potential formulation for simpler implementation. Taking the divergence of (3.20) and combining with (3.17) gives:

$$\nabla \cdot \mathbf{j} = \sigma_m \left(\nabla \cdot \mathbf{E} + \nabla \cdot (\mathbf{u} \times \mathbf{B}) \right) = 0 \tag{3.29}$$

A vector identity and (3.18) can simplify the last term:

$$\nabla \cdot (\mathbf{u} \times \mathbf{B}) = \mathbf{B} \cdot (\nabla \times \mathbf{u}) - \mathbf{u} \cdot (\nabla \times \mathbf{B}) = \mathbf{B} \cdot (\nabla \times \mathbf{u}) - \mu_0 \mathbf{u} \cdot \mathbf{j} = -\nabla \cdot \mathbf{E} \tag{3.30}$$

Putting (3.20) back into this equation gives:

$$-\nabla \cdot \mathbf{E} = \mathbf{B} \cdot (\nabla \times \mathbf{u}) - \mu_0 \sigma_m \mathbf{u} \cdot \mathbf{E} \tag{3.31}$$

Replacing the fields $\mathbf{E}$ and $\mathbf{B}$ with their potential formulations

$$\mathbf{E} = -\nabla V - \frac{\partial \mathbf{A}}{\partial t} \tag{3.32}$$

$$\mathbf{B} = \nabla \times \mathbf{A} \tag{3.33}$$

gives:

$$\nabla^2 V = (\nabla \times \mathbf{A}) \cdot (\nabla \times \mathbf{u}) + \mu_0 \sigma_m \mathbf{u} \cdot \left(\nabla V + \frac{\partial \mathbf{A}}{\partial t} \right) \tag{3.34}$$

As for the vector potential, taking (3.18) in its potential form simply gives[5]:

$$\nabla^2 \mathbf{A} = \mu_0 \sigma_m \left(\nabla V + \frac{\partial \mathbf{A}}{\partial t} - \mathbf{u} \times \nabla \times \mathbf{A} \right) \tag{3.35}$$

(3.34) and (3.35) can be used to perform bootstrap calculations of the electric and magnetic potential from one time step to the next.

3.4 Testing

OpenFOAM *solvers* are run on *cases*, dictionaries which contain information about the mesh, runtime controls and numerical algorithms.

3.4.1 OpenFOAM case structure

OpenFOAM is a free open-source collection of libraries and applications written in the C++ programming language designed to solve continuum mechanics problems[6]. It includes tools for mesh creation and manipulation as well as many numerical algorithms and discretisation schemes[5]. Each problem is run from a case directory with the following structure:

[5] In both cases the Coulomb gauge $\nabla \cdot \mathbf{A} = 0$ has been used to remove additional terms

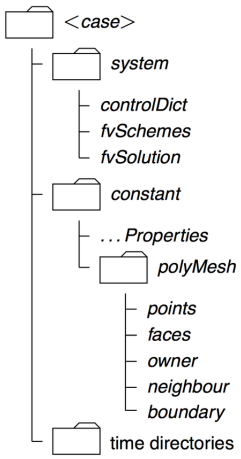

Figure 5: The file structure of an OpenFOAM case. The *polyMesh* directory contains all the information needed to create the mesh, while the time directories contain the field values at those times. The *Properties* files can be details of physical constants, thermophysical models, turbulence properties or any other information required by the solver. *controlDict* contains the runtime, time-step and output controls as well as the name of the solver used. *fvSchemes* defines the discretisation method for each term in the equations while *fvSolution* sets the algorithm and tolerances used in the numerical process.

Part II
Theory

4 Non-Linearity

The general procedure to investigate non-linear behaviour is to make a perturbative expansion in a quantity, and then compare orders in a Fourier transform of the governing equation of that quantity. We now follow this procedure[12][11], starting from charge continuity and non-viscous momentum balance. Fourier transforming (3.5) gives:

4.1 Non-Linear Density

$$-\omega\rho_k + \mathbf{k}\cdot\int d\lambda\rho_{k_1}\mathbf{u}_{k_2} = 0 \tag{4.1}$$

The shorthand notation:

$$d\lambda = dk_1dk_2\delta\left(k-k_1-k_2\right) = d\omega_1d\mathbf{k}_1d\omega_2d\mathbf{k}_2\delta\left(\omega-\omega_1-\omega_2\right)\delta\left(\mathbf{k}-\mathbf{k}_1-\mathbf{k}_2\right) \tag{4.2}$$

has been used. Expanding terms in a perturbation series $\rho_k = \rho_k^{(0)} + \rho_k^{(1)} + \rho_k^{(2)} + \ldots$, $\mathbf{u}_k = \mathbf{u}_k^{(1)} + \mathbf{u}_k^{(2)} + \ldots$, where the superscript indicates the polynomial dependence on the field and equating terms gives:

$$\rho_0\delta\left(k\right) = \rho_k^{(0)} \tag{4.3}$$

$$-\omega\rho_k^{(1)} + \rho_0\mathbf{k}\cdot\mathbf{u}_k^{(1)} \tag{4.4}$$

$$-\omega\rho_k^{(2)} + \rho_0\mathbf{k}\cdot\mathbf{u}_k^{(2)} + \mathbf{k}\cdot\int d\lambda\rho_k^{(1)}\mathbf{u}_k^{(2)} = 0 \tag{4.5}$$

4.2 Non-Linear Velocity

Applying the same process to (3.7) gives:

$$-i\rho_{k_1}\omega\mathbf{u}_k + i\int d\lambda\rho_{k_1}\left(\mathbf{u}_{k_1}\cdot\mathbf{k}_2\right)\mathbf{u}_{k_2} + ip_k\mathbf{k} = e\mathbf{E}_k + e\int d\lambda\mathbf{u}_{k_1}\times\mathbf{B}_{k_2} \quad (4.6)$$

The magnetic term can be removed by the Fourier transform of (3.12):

$$\mathbf{k}\times\mathbf{E}_k = \omega\mathbf{B}_k \quad (4.7)$$

$$\mathbf{u}_{k_1}\times\mathbf{B}_{k_2} = \frac{1}{\omega_2}\mathbf{u}_{k_1}\times\mathbf{k}_2\times\mathbf{E}_{\mathbf{2}k} = \frac{\mathbf{k}_2}{\omega_2}\left(\mathbf{u}_{k_1}\cdot\mathbf{E}_{k_2}\right) - \frac{\mathbf{E}_{k_2}}{\omega_2}\left(\mathbf{k}_2\cdot\mathbf{u}_{k_1}\right) \quad (4.8)$$

These terms are all at least second order. Looking at first order terms in (4.6) gives:

$$\rho_0\omega\mathbf{u}_k^{(1)} = p_k\mathbf{k} + ie\mathbf{E}_k \quad (4.9)$$

In the regime where the thermal energy is small we can neglect the pressure term.[6]
To second order, the last term in (4.8) cancels exactly with the third term in (4.6) because of (4.9). This leaves:

$$\mathbf{u}_k^{(2)} = \frac{ie}{\rho_0\omega}\int d\lambda\frac{\mathbf{k}_2}{\omega_2}\left(\mathbf{u}_{k_1}^{(1)}\cdot\mathbf{E}_{k_2}\right) = -\frac{e^2}{\rho_0^2\omega}\int d\lambda\frac{\mathbf{k}_2}{\omega_2\omega_1}\left(\mathbf{E}_{k_1}\cdot\mathbf{E}_{k_2}\right) \quad (4.10)$$

$$= -\frac{e^2}{2\rho_0^2\omega}\int d\lambda\frac{\mathbf{k}}{\omega_2\omega_1}\left(\mathbf{E}_{k_1}\cdot\mathbf{E}_{k_2}\right) \quad (4.11)$$

where in the last step $\mathbf{k}_2$ has been replaced by $\frac{\mathbf{k}}{2}$, which can be done since it is symmetric under interchange of the two indices.
σ obeys a continuity equation identical to ρ, therefore the analysis in 4.1 is applicable:

$$\sigma_0\delta\left(k\right) = \sigma_k^{(0)} \quad (4.12) \qquad -\omega\sigma_k^{(1)} + \sigma_0\mathbf{k}\cdot\mathbf{u}_k^{(1)} \quad (4.13)$$

$$-\omega\sigma_k^{(2)} + \sigma_0\mathbf{k}\cdot\mathbf{u}_k^{(2)} + \mathbf{k}\cdot\int d\lambda\sigma_k^{(1)}\mathbf{u}_k^{(2)} = 0 \quad (4.14)$$

From (4.9) and (4.13) we have:

$$\sigma_k^{(1)} = \frac{ie^2}{m_e\omega^2}\mathbf{k}\cdot\mathbf{E}_k \quad (4.15)$$

First order perturbations to charge density therefore only arise from *longitudinal* waves. The phase velocity of these electron acoustic waves is much larger than the thermal velocity. Ion acoustic waves can occur when the electrons are at a

[6]Such regimes are known as cold plasmas, they are characterised by the thermal velocity being much smaller than the phase velocity i.e. $\sqrt{T} \ll \frac{\omega}{k}$

much higher temperature than the ions. Their phase velocity will then be much less than the electron thermal velocity, but much higher than the ion thermal velocity. Non-linear i.e. second order perturbations can arise from transverse waves. From (4.10) and (4.14) with $-\omega\sigma_k^{(1)} = 0$:

$$\sigma_k^{(2)} = -\frac{e^2k^2}{2\rho_0^2\omega^2}\int \frac{d\lambda}{\omega_2\omega_1}\left(\mathbf{E}_{k_1}\cdot\mathbf{E}_{k_2}\right) \tag{4.16}$$

4.3 Non-Linear Current

Fourier transforming (3.4) gives:

$$\mathbf{j}_k = (\sigma\mathbf{u})_k = \int d\lambda\sigma_{k_1}\mathbf{u}_{k_2} \tag{4.17}$$

As before, make a perturbative expansion $\mathbf{j}_k = \mathbf{j}_k^{(1)} + \mathbf{j}_k^{(2)} + \ldots$:

$$\mathbf{j}_k^{(1)} = \int d\lambda\sigma_{k_1}^{(0)}\mathbf{u}_{k_2}^{(1)} = \sigma_0\mathbf{u}_k^{(1)} = \frac{ie^2}{m_e\omega_k}\mathbf{E}_k \tag{4.18}$$

where $\frac{\sigma_0}{\rho_0} = \frac{e}{m_e}$ and (4.9) have been used in the last step. The first order term recreates Ohm's Law. Now for the second order terms:

$$\mathbf{j}_k^{(2)} = \int d\lambda\left(\sigma_{k_1}^{(0)}\mathbf{u}_{k_2}^{(2)} + \sigma_{k_1}^{(1)}\mathbf{u}_{k_2}^{(1)}\right) \tag{4.19}$$

The first term can be evaluated using (4.12) and (4.10):

$$\int d\lambda\sigma_{k_1}^{(0)}\mathbf{u}_{k_2}^{(2)} = \sigma_0\mathbf{u}_k^{(2)} = -\frac{\sigma_0e^2}{2\rho_0^2\omega}\int d\lambda\frac{\mathbf{k}}{\omega_2\omega_1}\left(\mathbf{E}_{k_1}\cdot\mathbf{E}_{k_2}\right) \tag{4.20}$$

The second term can be evaluated using (4.13) and (4.9):

$$\int d\lambda\sigma_{k_1}^{(1)}\mathbf{u}_{k_2}^{(1)} = \frac{ie\sigma_0}{\rho_0}\int\frac{d\lambda}{\omega_1^2\omega_2}\left(\mathbf{k}_1\cdot\mathbf{u}_{k_1}^{(1)}\right)\mathbf{E}_{k_2} = -\frac{e^2\sigma_0}{\rho_0^2}\int\frac{d\lambda}{\omega_1^2\omega_2}\left(\mathbf{k}_1\cdot\mathbf{E}_{k_1}\right)\mathbf{E}_{k_2} \tag{4.21}$$

This can be symmetrised by letting $\mathbf{k}_1 = \mathbf{k}_2 = \frac{\mathbf{k}}{2}$ Together:

$$\mathbf{j}_k^{(2)} = -\frac{e^2\sigma_0}{2\rho_0^2}\int\frac{d\lambda}{\omega_1^2\omega_2}\left[\frac{\mathbf{E}_{k_1}\cdot\mathbf{E}_{k_2}}{\omega}\mathbf{k} + \mathbf{E}_{k_2}\frac{\mathbf{k}_1\cdot\mathbf{E}_{k_1}}{\omega_1} + \mathbf{E}_{k_1}\frac{\mathbf{k}_2\cdot\mathbf{E}_{k_2}}{\omega_2}\right] \tag{4.22}$$

The last two terms got to zero when the wavevector $\mathbf{k}$ is perpendicular to the amplitude $\mathbf{E}_k$. They arise from the plasma current carried by (longitudinally generated) charge density waves rather than the electromagnetic waves.

5 Landau Kinetic Theory

So far, the treatment has either assumed a Maxwell-Boltzmann distribution, bypassed the need to involve the distribution. Kinetic theory is required when we can do neither of these things. The cornerstone of kinetic theory is the Vlasov equation for the particle distribution function $f(\mathbf{x}, \mathbf{u}, t)$:

$$\frac{\partial f}{\partial t} + \mathbf{u} \cdot \nabla f + \frac{q}{m} (\mathbf{E} + \mathbf{u} \times \mathbf{B}) \cdot \frac{\partial f}{\partial \mathbf{u}} = 0 \tag{5.1}$$

In the analysis that follows we will assume that the magnetic field is either small or parallel to any motion. Landau's approach is to write the distribution function as[4] (in 1D):

$$f(x, u, t) = f_0(u) + f_1(u, t)) \exp(ikx) \tag{5.2}$$

We assume a solution of spatially varying normal modes $fE(t)) \exp(ikx)$ around a flat initial distribution function f_0
The Vlasov equation for electrons now becomes:

$$\frac{\partial f_1}{\partial t} + iku f_1 - \frac{e}{m_e} E \frac{\partial f_0}{\partial u} = 0 \tag{5.3}$$

Employing the method of Laplace transformation with:

$$\tilde{f}_1(u, s) = \int_0^\infty f_1(u, t) e^{-st} dt \tag{5.4}$$

and the time derivative rule $\tilde{\dot{f}} = s\tilde{f}(s) - f(0)$

$$(s + iku) \tilde{f}_1(u, s) = f_1(u, 0) + \frac{e}{m_e} \tilde{E}(s) \frac{\partial f_0}{\partial u} \tag{5.5}$$

Gauss' law can also be Laplace transformed:

$$ik\epsilon_0 \tilde{E}(s) = -e \int_{-\infty}^{\infty} \tilde{f}_1(vu, s) du \tag{5.6}$$

Now:

$$\left[1 - \frac{ie^2}{m_e \epsilon_0 k} \int_{-\infty}^{\infty} \frac{\partial f_0 / \partial u}{s + iku} du\right] \tilde{E}(s) = \frac{ie}{\epsilon_0 k} \int_{-\infty}^{\infty} \frac{f_1(u, 0)}{s + iku} du \equiv D(k, s) \tilde{E}(s) \tag{5.7}$$

$D(f, s)$ is the plasma dielectric function.
To recover $E(t)$ we require the Laplace inversion formula:

$$E(t) = \frac{1}{2\pi i} \int_{-i\infty + s_0}^{i\infty + s_0} \tilde{E}(s) e^{st} ds \tag{5.8}$$

where s_0 is chosen such that the so-called Bromwich contour lies to the right of all singularities. This is a contour integral and as such is equivalent to the sum of the residues of $\tilde{E}(s) e^{st}$. It can be shown that all singularities of interest[7] arise from zeroes of the dielectric function. The behaviour of $E(t)$ as $t \longrightarrow \infty$ is found by shifting the inversion contour as far left as possible without hitting a singularity. The dominant contribution comes from the first singularity.

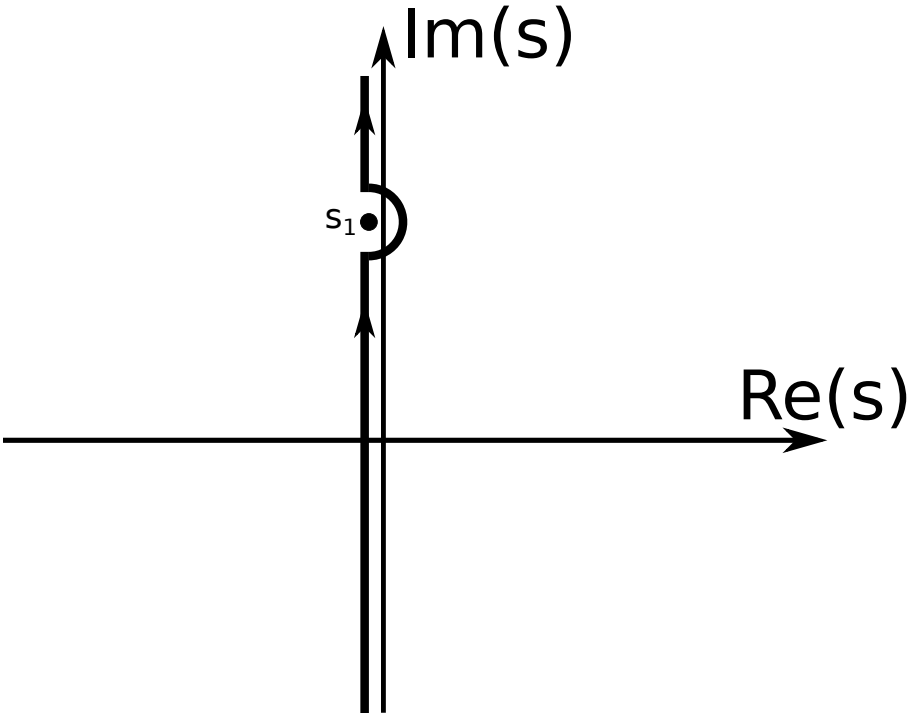

Figure 6: The Bromwich contour runs along the imaginary axis with a small semicircular detour around the singularity s_1

5.1 Landau Damping

Landau damping occurs when the first (i.e. right-most) singularity has a small, negative real part.
To frame in more physical terms we make a transformation $s_1 = -i\omega$. The dielectric function then takes the form of a dispersion relation:

$$D(k,\omega) = 1 + \frac{e^2}{m_e \epsilon_0 k}\left(\int_{-\infty}^{\infty} \frac{\partial f_0/\partial u}{s + iku} du - \frac{i\pi}{k}\left.\frac{\partial f_0}{\partial u}\right|_{u=\omega/k}\right) \tag{5.9}$$

where the last term is a result of the detour. In the case of a Maxwell-Boltzmann distribution:

$$f_0 = \left(\frac{n^2 m}{2\pi k_B T}\right)^{\frac{1}{2}} \exp\left(-\frac{mu^2}{2k_B T}\right) \tag{5.10}$$

and making the expansion

$$\frac{1}{\omega - ku} = \frac{1}{\omega} + \frac{ku}{\omega^2} + \frac{k^2u^2}{\omega^3} + \frac{k^3u^3}{\omega^4} + \dots \tag{5.11}$$

[7] Other singularities can exist which describe damping of the initial velocity distribution $f_1(u,0)$ but these do not affect this discussion.

$$D = 1 - \frac{\omega_p^2}{\omega^2}\left(1 + \frac{3k_BT}{m}\frac{k^2}{\omega^2}\right) + i\left(\frac{\pi m^3}{2\left(k_BT\right)^3}\right)^{\frac{1}{2}} \frac{\omega_p^2\omega}{k^3} \exp\left(-\frac{m\omega^2}{2k_BTk^2}\right) \quad (5.12)$$

As per the previous discussion, the dominant behaviour comes from the zeroes of D.. Solving $D = 0$ gives the dispersion relation.[8]

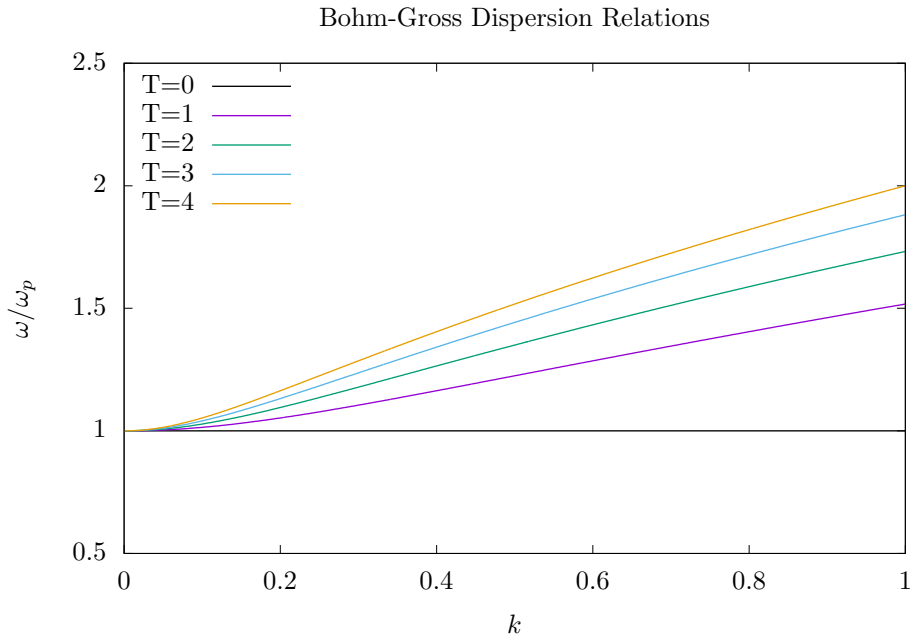

Figure 7: The Bohm-Gross dispersion relation[2] is $\omega^2 = \omega_p^2 + 3\frac{k^2T}{m}$ but there are small thermal corrections particularly evident at high wavevectors.
The imaginary part of the dielectric function quantifies the damping. Landau damping occurs regardless of whether there are collisions.

5.1.1 Inverse Damping

If we assume that the imaginary part of (5.7) is small, then the approximate dispersion relation is:

$$\omega = \omega_p + i\frac{\pi\omega_p^3}{2nk^2}\left.\frac{\partial f_0}{\partial u}\right|_{u=\omega/k} \quad (5.13)$$

For most distributions, such as the Maxwell-Boltzmann distribution, the imaginary term is always negative at resonance since there are generally fewer fast particles than slow ones. However, in the case that a distribution function has a double peak then $\frac{\partial f_0}{\partial u}$ can be positive at $u = \omega/k$. Instead of damping there is exponential growth and instability as waves gain energy from the resonant particles.

[8] ω_p has the usual definition $\omega_p = \frac{ne^2}{m\epsilon_0}$

6 Conclusion

Three models of plasma were examined; two from a computational viewpoint and the the third with a theoretical approach. The particle-in-cell model was found to work well in the presence of strong fields, such as in the magnetic bottle. At high thermal velocities, the discretisation limits the accuracy since particles may move across many cell boundaries in a single timestep. Kinetic theory was applied to a few problems; both Tsytovich and Landau's treatment have their merits.

6.1 Further Work

The particle-in-cell software was very successful, however it can undoubtedly be made faster given enough time to apply more advance code optimisation techniques. Once this is done it would be interesting to test it in scenarios with more particles, more objects, finer graded lattice and a longer run-time. It has also left open the option to try out higher order weight functions and different deposition procedures. There is a huge range of possible applications for the OpenFOAM solver; it was only really tested to check it worked, without exploiting the power of the numerical techniques employed. There are many more non-linear phenomena which were not touched on in the theory section which arise from thermal gradients.

References

[1] Stephen J. Blundell and Katherine M. Blundell. *Concepts in Thermal Physics*. 2010.

[2] D. Bohm and E. P. Gross. "Theory of Plasma Oscillations. A. Origin of Medium-Like Behavior". In: *Phys. Rev.* (1949).

[3] J. Boris. In: *Proceedings of the Fourth Conference on Numerical Simulation of Plasmas* (1970).

[4] Robert J. Goldston and Paul H. Rutherford. *Introduction to Plasma Physics*. 1970.

[5] Christopher J. Greenshields. *OpenFoam Programmer's Guide*. 2015.

[6] Christopher J. Greenshields. *OpenFoam User's Guide*. 2015.

[7] A. A. Harms et al. *Principles of Fusion Energy*. 2000.

[8] G. Lapenta. *A brief description of the PIC Method*. 2010.

[9] Javier Luis Lopez. "Coil off axis magnetic field using elliptic integrals and Maxwell method with C++ code". In: (2014).

[10] M. Mitchner and Charles H. Kruger Jr. *Partially Ionized Gases*. 1973.

[11] Vadim N.Tsytovich. *Lectures on Non-Linear Plasma Kinetics*. 1995.

[12] Vadim N.Tsytovich. *Nonlinear Effects in Plasma*. 1970.

[13] H. Qin et al. *Why is Boris algorithm so good?* 2013.

[14] F. Rossi. "Development of algorithms for an electromagnetic particle in cell code and implementation on a hybrid architecture (CPU+GPU)". University of Bologna, 2011.

[15] M. Sass-Tisovskaya. "Plasma Arc Welding Simulation with OpenFOAM". Chalmers University of Technology, 2009.

[16] I.P. Shkarofsky, T.W. Johnston, and M.P. Bachynski. *The Particle Kinetics of Plasmas*. 1966.

[17] T. Umeda et al. "A new charge conservation method in electromagnetic particle-in-cell simulations". In: *Comput. Phys. Comm.* (2003).

[18] K.S. Yee. "Numerical Solution of Initial Boundary Value Problems Involving Maxwells Equations in Isotropic Media". In: *IEEE Trans. Antennas Prop.* (1966).

[19] Esirkepov T. Zh. "Exact charge conservation scheme for Particle-in-Cell simulation with an arbitrary form-factor". In: *Comput. Phys. Comm.* (2000).

[20] J. Martin van Zyl. "Testing for normality using the cumulant generating function". In: (2015).

Appendices

7 Appendix A

The memory stick contents:

- All the particle-in-cell source code and header files
- Gnuplot scripts for making gifs and images
- The makefile for the program
- A collection of plots and gifs
- The OpenFOAM solver
- Digital copies of this document